






Flow Distribution in Molten Salt Receiver Panels at High Flux Gradients

Investigating the Risk of Stagnating Flow Due to Uneven Irradiation

Christian Schwager¹ , Jonas Schulte^{1,*} , Matthias Binder² ,
Cristiano José Teixeira Boura¹ , and Ulf Herrmann¹ 

¹ Solar-Institut Jülich of FH Aachen University of Applied Sciences, Germany

² MAN Energy Solutions SE, Germany

*Correspondence: j.schulte@sj.fh-aachen.de

Abstract. This paper presents a simulation study on critical mass flow distributions in receiver panels of commercial-scale molten salt towers (MST). Despite sophisticated aimpoint optimizations, the flux density distribution on an MST receiver in actual operation contains significant vertical and horizontal gradients. This study investigated how the latter affects the mass flow distribution among the parallel absorber tubes in each panel. A parametric study applied a discretized dynamic thermohydraulic model of a commercial scale receiver design, highlighting at which mass flow rates, flux density gradients and mean flux densities the flow distribution can become critical. Excessive temperature developments were observed, suggesting maintaining appropriate minimal mass flow rates to avoid damaging tube walls and the molten salt chemistry.

Keywords: Molten Salt Tower, Dynamic Simulation, Critical Operation, Mass Flow Control

1. Introduction

Molten salt towers (MST) have become a state-of-the-art technology for efficiently harnessing solar energy with integrated energy storage. Developers and researchers keep pushing the limits to increase efficiency and reduce the levelized cost of the produced electricity. Consequently, the core components of the molten salt solar receiver must operate close to its physical limits. Besides conventional limits for material and heat transfer fluid (HTF) temperatures, more sophisticated operational limitations have been introduced tailored to this technology. For example, Vant-Hull [1] introduced the concept of allowable flux density (AFD) limits based on maximum HTF film temperature and thermal stress limitations, which are commonly applied in MST engineering. More recently, Binder *et al.* [2] and Hering *et al.* [3] developed methods to predict the lifetime consumption of absorber tubes due to their uneven and transient irradiation. Also, Popp *et al.* [4] tackled the challenging dynamic behavior of an MST receiver with a model predictive controller that limits local film temperature peaks by proactively adjusting the HTF mass flow rate.

However, those approaches consider even HTF flow distribution within each receiver panel. Commercial-scale MST receivers are composed of several panels connected in series, which each hold a bundle of parallel absorber tubes, as illustrated in Figure 1. Hence, the overall HTF flow splits into numerous tube flows in each receiver panel. Without any solar flux,

the flow distribution should be more or less even since the header volumes are designed appropriately large so that the wall friction inside the absorber tubes dominates the pressure loss and, therefore, the mass flow rates. When the tubes heat up by the concentrated solar radiation and the heat is transferred to the HTF, it affects the fluid properties. Especially the HTF density varies by approximately 10 % in the operational temperature range, impacting the gravitational force on the fluid column in each absorber tube. At the same time, due to the sun's position, the heliostat field layout and (sometimes) partial shading, the solar flux density is not distributed homogeneously onto the receiver. Instead, the flux density distribution has horizontal (circumferential on the cylindrical receiver surface) and vertical gradients, even in clear-sky conditions [5].

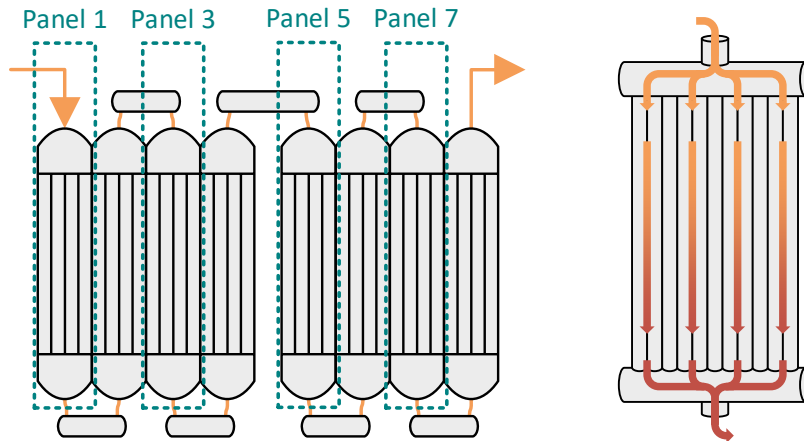


Figure 1. The flow pattern through a receiver flow path (half of the receiver) and an exemplary (downstream) receiver panel.

Consequently, the HTF in the tubes with higher flux density is heated to higher temperatures and thus has a lower density compared to the HTF in less irradiated tubes. This has a self-regulating effect in upstream panels (inlet at the bottom) since the lowered density causes the flow in the high flux areas to increase. In contrast, this poses a self-reinforcing effect for downstream panels (inlet at the top), which can significantly decrease the HTF flow in high flux areas and even cause natural circulation between different tubes within one panel. This study investigates with the help of dynamic process simulation in which operational regimes this critical phenomenon can occur to derive potential consequences for safe control strategies.

2. Approach

Based on previously developed and validated dynamic models [6], a simulation setup is implemented in the modeling language Modelica, representing a single receiver panel of a commercial-scale (external, cylindrical) molten salt receiver. Typical for this type of solar tower, the receiver is subdivided into two individually controlled parallel flow paths consisting of several panels in series. To minimize computing time, each simulation only considers one of the 8 receiver panels (per flow path). The Panel model is parametrized for each downstream panel according to the design specifications in Table 1. In this model, the absorber tube wall has axial, radial and circumferential discretization to account for any significant temperature gradients. The fluid flow has only vertical discretization with additional non-differential equations for determining the maximum fluid film temperature at the front side (crown) along each tube (as presented by Schwager *et al.* [6]). For appropriate computing performance, the model only solves the differential equations of one representative (simulated) tube for every four (real) absorber tubes. This ratio (13 simulated tubes), as well as the level of axial discretization (16 axial tube wall and flow elements), is chosen based on a grid independence study, as shown in Figure 2. Moreover, lumped volume models represent the top and bottom header to describe the dynamic mixing of differently heated HTF. The inlet mass flow rate and temperature is

prescribed either according to Table 1 (in scenario 1 and 2) or changed step-wise (in scenario 0).

Table 1. Receiver design specifications.

Parameter	Unit	Panel 1	Panel 3	Panel 5	Panel 7
Nom. panel inlet temperature	°C	290	381	466	529
Nom. panel outlet temperature	°C	335	421	502	549
Max. allowable film temperature	°C	600			
Nom. receiver power	[MW _{th}]	2 · 350			
Nom. receiver mass flow rate	[kg/s]	2 · 828.5			
Number of parallel flow paths	-	2			
Number of receiver panels	-	2 · 8			
Number of absorber tubes per panel	-	52			
Absorber tube outer diameter	mm	60.3			
Absorber tube radiated length	m	19.8			

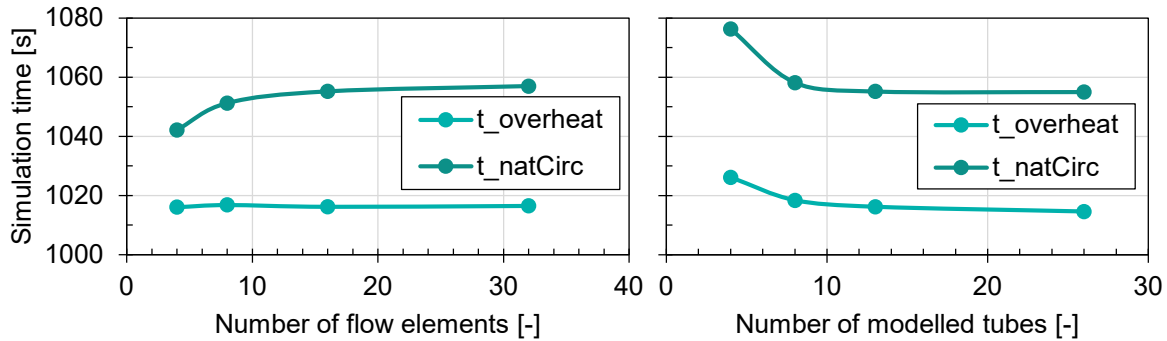


Figure 2. Grid dependence of the overheating and natural circulation delays (comp. section 3.2) for the axial discretization (number of flow elements) and number of simulated tubes.

3. Scenarios and Results

3.1 Test – Scenario 0

The purpose of this first test scenario is to observe the transition from even flow distribution to stagnation and natural circulation caused by a specific flux gradient under different mass flow rates. For this, the simulation is set up to represent panel 5 with a constant inlet temperature of 466 °C starting with a 24 % mass flow rate (of nominal flow path mass flow rate) and a homogeneous flux density of 238 kW/m². In this condition, the HTF flow naturally distributes evenly across all absorber tubes. After 500 s, a linear horizontal flux gradient of approx. 75 (kW/m²)/m is applied as shading on the flux density distribution. As shown in Figure 3, the last four tubes are nearly fully shaded, and the first four tubes are nearly unshaded. In between, the flux density gradually increases from each to the next tube. The vertical flux gradient remains zero. This flux distribution is fixed throughout the remaining simulation time. The mass flow rate is reduced in two steps: first to 22 % of the nominal value at 1000 s and second to 15 % at 1500 s. In between, the (overall) mass flow rate through the receiver panel is constant.

As expected, the panel outlet temperature plotted in Figure 4 drops at 500 s due to the decreased solar flux and slightly increases due to the reduced mass flow rate after 1000 s. However, after the second flow reduction at 1500 s, the outlet temperature becomes unstable while the maximum film temperature in the panel reaches extremely high values. This can be explained by the individual tube mass flow rates. As soon as the flux gradient is applied, the mass flow rates drift apart and first settle in a range between 21 % and 27 %, even though the

overall mass flow rate remains constant. This is due to the more dense HTF in the less irradiated, thus colder, tubes in contrast to the less dense HTF in the unshaded, thus hotter, tubes. Since a decrease in the flow rate causes the HTF temperature to rise even higher, this phenomenon is self-reinforcing and develops over time. It appears to stabilize as soon as the increased friction pressure loss balances the increased geodetic pressure. The overall flow rate reduction after 1000 s intensifies this effect since the friction pressure loss decreases, making the geodetic pressure difference more significant. At 15% relative (overall) mass flow rate, the flow distribution becomes unstable so that the flow direction in the first representative tube (1...4) flips, followed by the second and third (5...8 and 9...12). Whenever the flow rate in a tube crosses zero, the corresponding local film temperatures peak due to insufficient cooling, which explains the excessive peaks in the overall maximum film temperature trend.

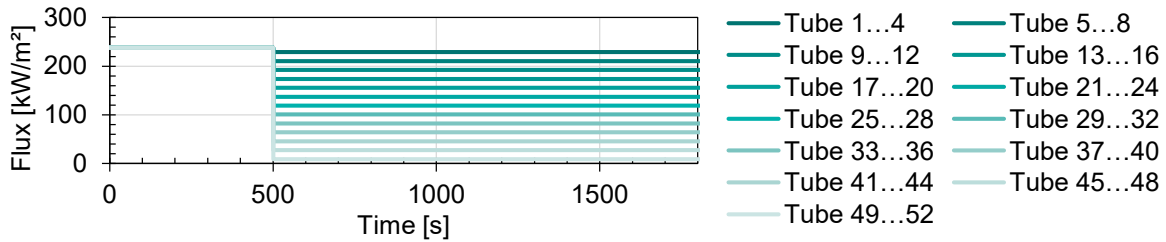


Figure 3. Flux density trends on each absorber tube.

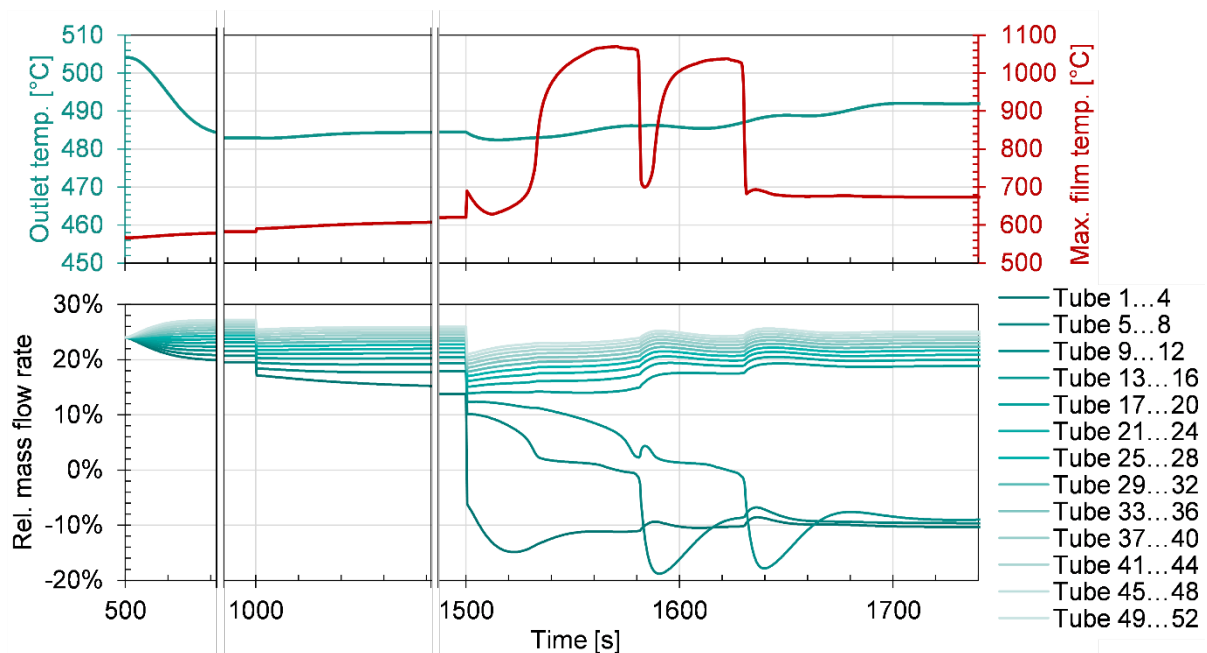


Figure 4. Temperature and mass flow rate trends across the entire panel in scenario 0.

Moreover, Figure 5 reveals the bulk temperature profile in the first two simulated tubes. It can be observed how the temperature profile spreads out due to the flow reduction and completely flips after the panel becomes hydraulically unstable. Only in the first tube (1...4) the flow flips almost instantly, whereas the second tube (5...8) is subject to a delay of approx. 80 s. Also, for about 50 s before the flip, the temperature rise appears to be decelerated. This is due to the drastically inhibited heat transfer in the laminar flow regime. Accordingly, the HTF receives less heat input, but the film temperature, which is linked to the tube wall, experiences a steep incline, as shown in Figure 4. Approximately 200 s after the last external change, the tubes then reach a new steady state, in which the flow in some tubes remains reversed, establishing natural circulation within this receiver panel. As shown in Figure 4, this steady state still results in excessively high film temperatures. However, the most extreme peaks occur when the HTF flow flips and nearly stagnates for a moment.

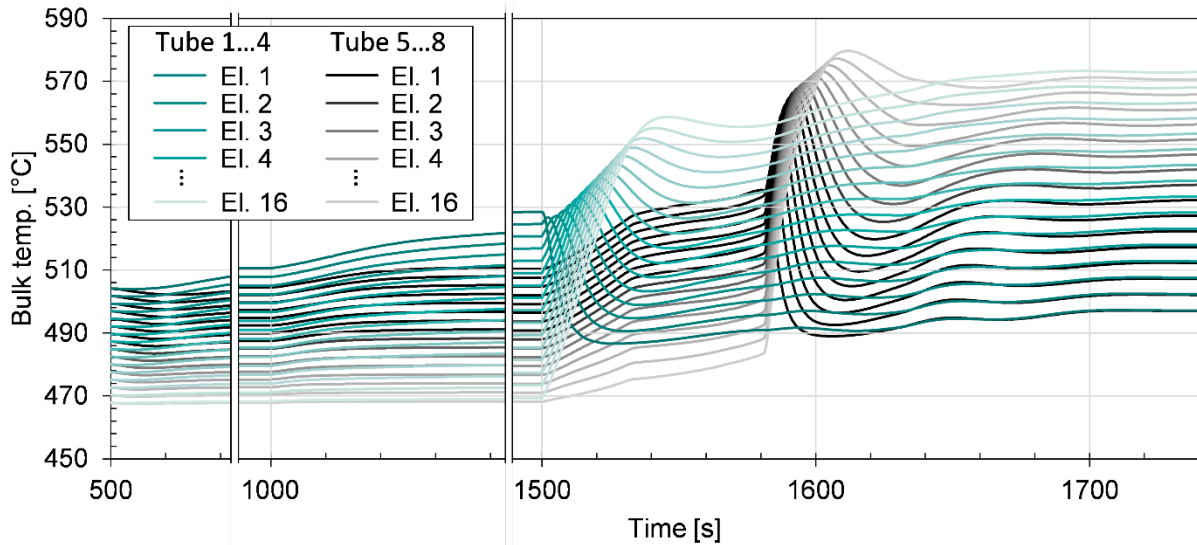


Figure 5. Flow-element-wise bulk temperature trends in the absorber tubes 1...4 and 5...8.

3.2 Parametric study – Scenario 1 & Scenario 2

To evaluate the significance of this phenomenon for daily operation, a parametric study is conducted across the three impact factors: overall flux, flux gradient and HTF flow rate. Simulations are performed for all downstream panels (1, 3, 5 and 7). More specifically, the panel mass flow rate is varied in 2.5 percentage point increments between 10 % and 30 %. Since it would be unnecessary to simulate a very high mass flow rate with a very low flux and vice versa, the mean flux density is adjusted each time to achieve the panel's nominal outlet temperature. This reduces the 3D parameter space to a 2D space. However, the results can only be accounted relevant if these simulations comply with the allowable flux density (AFD) limits. These account for local film temperatures and thermal stress limits depending on HTF temperature and flow rate, as shown in Figure 6.

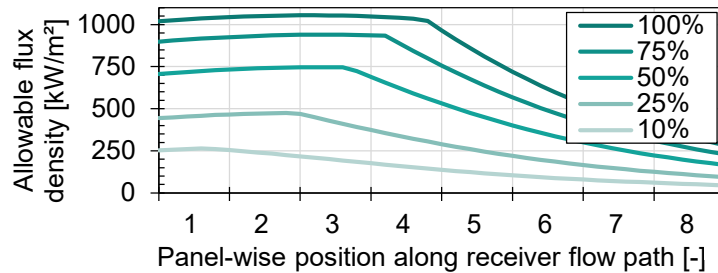


Figure 6. Considered AFD limits for relative mass flow rates from 10 % to 100 %.

In this context, two different scenarios are considered. The simulation is initialized in both with no horizontal flux gradient (zero flux density spread). The vertical flux gradient correlates with the AFD at the inlet and outlet of the considered panel with a linear profile in between. In scenario 1, the entire flux distribution is scaled to achieve the nominal outlet temperature (in steady state). After 2000 s, the horizontal flux gradient is added. If the resulting flux density distribution exceeds the AFD then it is shifted down as far as necessary to comply with the AFD limit. As shown in Figure 7 (left), this approach maintains a constant mean value as long as the AFD is not exceeded. However, this scenario represents a semi-steady-state control where the controller always tries to achieve the nominal temperature lift. A sophisticated (more aggressive) model predictive controller (MPC) might temporarily increase the temperature lift of a panel (by further mass flow rate reduction) to make up for previous flux deficits (due to clouds). This brings the panel flux closer to the AFD limit than it is considered in scenario 1. Therefore, the flux density distributions in scenario 2 are always maximized to the AFD as shown in Figure 7 (right). In both scenarios, the flux density spread is defined as the relative

flux difference between the most outer tubes. It instantly switches from zero to the designated value at 2000 s simulation time.

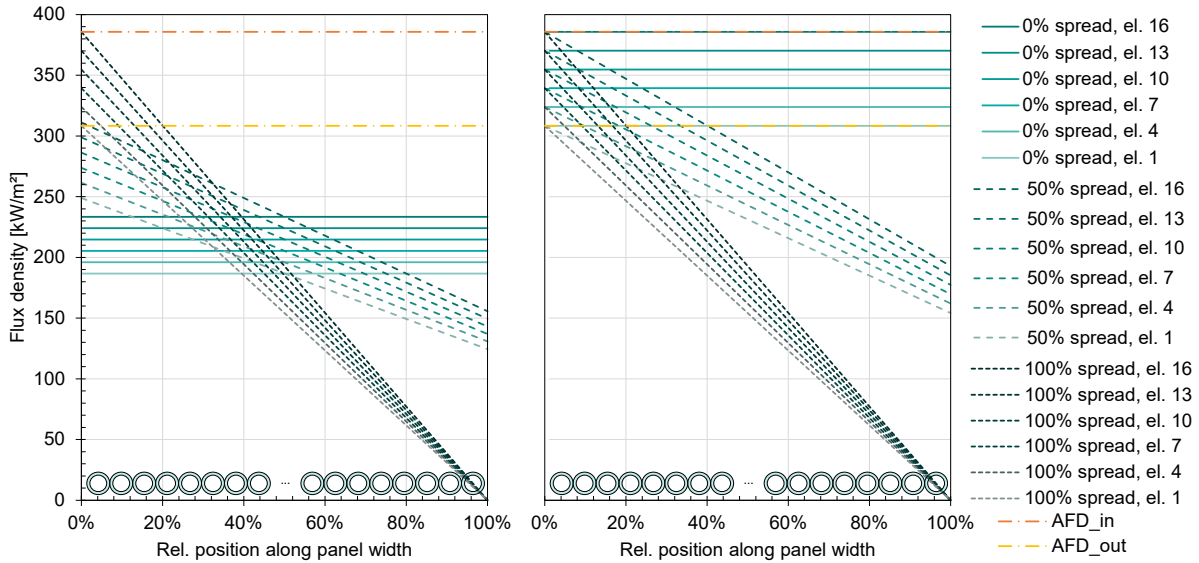


Figure 7. Illustration of the flux density distribution depending on different spreads (relative horizontal flux density gradient) in scenario 1 (left) and scenario 2 (right).

The resulting mean flux values for scenario 1 are presented in Figure 8, as well as the minimal deviation of the actual flux density from the corresponding AFD. For panels 1, 3 and 5, the flux stays far below the AFD and the gap disappears with higher flux spreads. Due to higher temperatures, panel 7 always operates at the AFD limit.

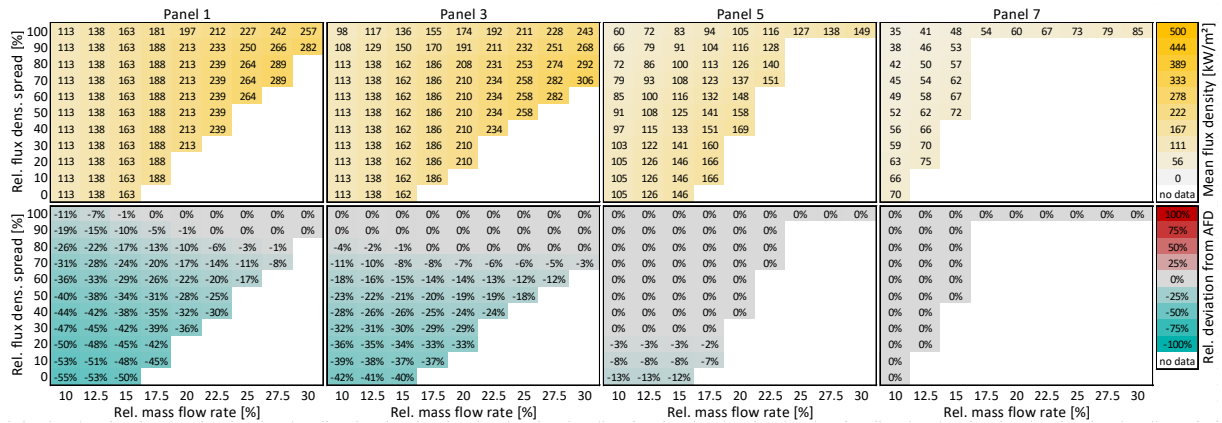


Figure 8. Mean flux densities and corresponding min. flux deviation from AFD in scenario 1.

Finally, Figure 9 reveals under which operational conditions the simulations predict critical states. The top plots show the delay between the flux spread application until any tube reaches zero mass flow rate, hence the start of natural circulation. The bottom plots show the highest observed local film temperature during this simulation. Delays of more than 300 s are considered less critical (green shading) since this could provide sufficient time for counteractions. However, the results show significant numbers of occurrences, especially in high flux panels 1 and 3. At mass flow rates below 20 %, natural circulation can be triggered even by very mild flux spreads, and at 10 % mass flow rate, even without any spread (see 0 s values). This can be explained by the self-reinforcing buoyancy effect coupled with relatively low friction forces. In some rare cases, excessive film temperatures can be observed even without any natural circulation just due to the reduced flow rate on the high flux side of the panel. As expected, the higher flux densities in scenario 2 result in shorter delays, higher peak temperatures and consequently an enlargement of the critical regime (see Figure 10).

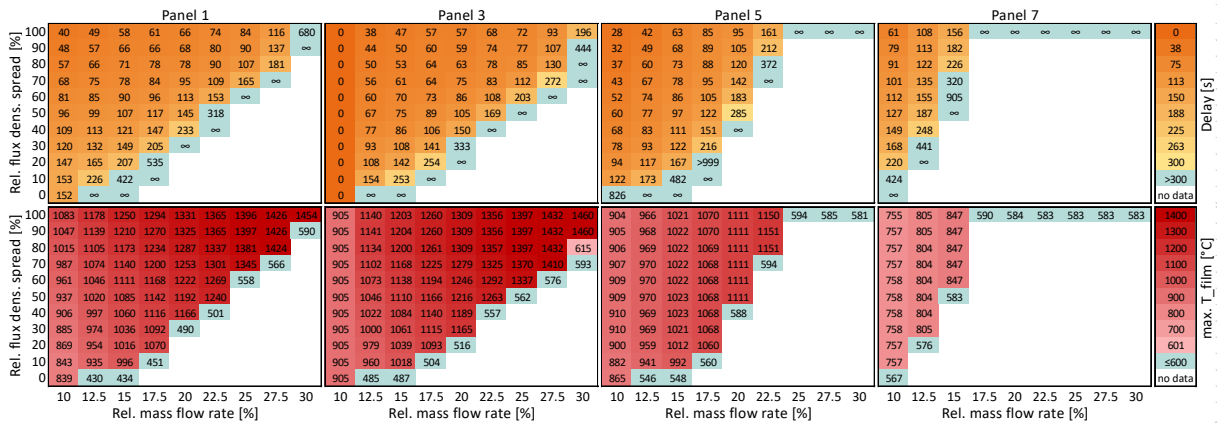


Figure 9. The resulting natural circulation delays and film temp peak values in scenario 1.

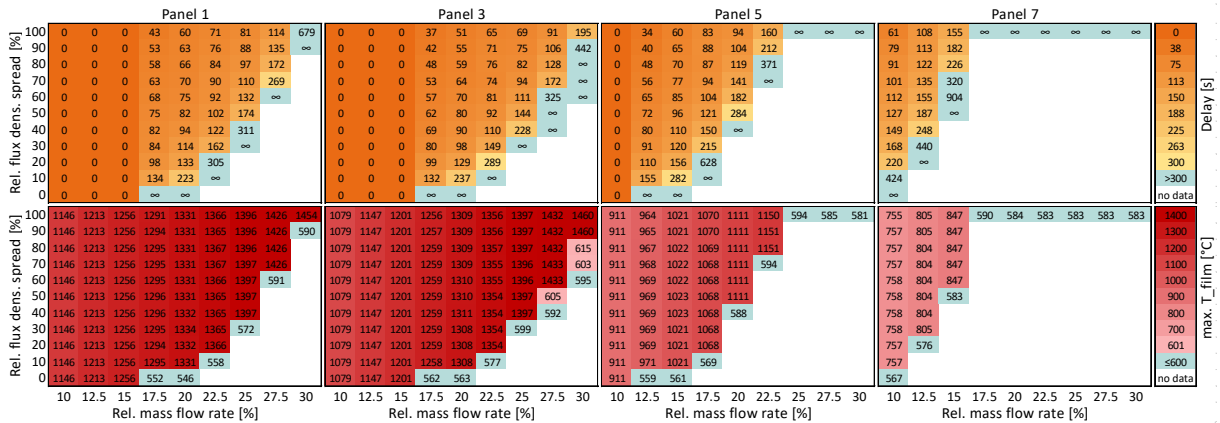


Figure 10. The resulting natural circulation delays and film temp peak values in scenario 2.

To put the results into perspective, simulations based on measured DNI maps are performed for one exemplary day. Accordingly, the cumulative probability in Figure 11 indicates how often certain flux spreads are observed. For instance, 25 % of the time, the flux spread on panel 5 is higher than 20 %, underlining the significance of the above-discussed results.

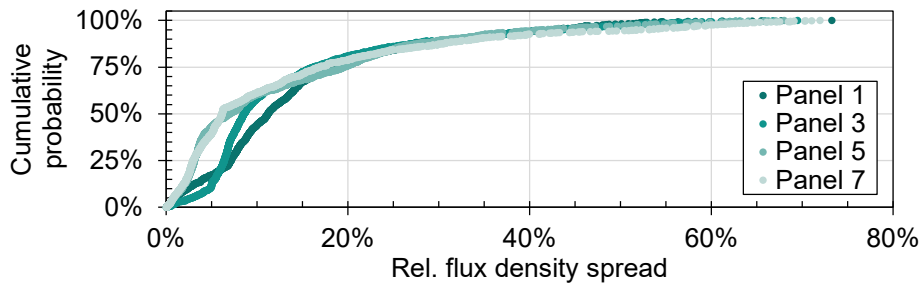


Figure 11. Cumulative distribution plot for the flux spreads based on all-sky imager-based DNI measurements and raytracing simulation (from 6 Sep. 2019 in Almeria) [7].

4. Conclusion and Outlook

A parametric study was conducted using detailed dynamic process simulations to investigate the risk of flux-gradient-induced natural circulation and resulting peak temperatures in MST receiver panels. The results indicate that critical mass flow imbalances can occur under solar flux values in the allowable range, at mass flow rates below 30 % and especially at high horizontal flux gradients (flux spread). Below 17.5 % mass flow rate, even mild flux gradients can cause the mass flow rate to diverge enough, causing critical temperature peaks. Upcoming research should investigate the influence of different panel designs (height-to-width ratio and

tube diameter) and pressure-loss-impacting features such as individual tube bends and weldings. Further putting this into practical application, instead of setting conservatively high mass flow rate limits, it is recommended to develop further a model predictive intelligence allowing for safer and still efficient operation.

Data availability statement

The applied data are subject to third-party IP and unavailable to the public.

Author contributions

C. Schwager: Conceptualization, Data curation, Formal Analysis, Funding acquisition, Investigation, Methodology, Project administration, Software, Visualization, Writing – original draft, Writing – review & editing; **J. Schulte:** Writing – review & editing; **M. Binder:** Data curation, Writing – review & editing; **C. J. T. Boura:** Funding acquisition, Supervision, Writing – review & editing; **U. Herrmann:** Funding acquisition, Supervision, Writing – review & editing

Competing interests

The authors declare no competing interests.

Funding

This work is funded by the German Federal Ministry for Economic Affairs and Climate Action.

References

- [1] L. L. Vant-Hull, "The Role of "Allowable Flux Density" in the Design and Operation of Molten-Salt Solar Central Receivers," *J. Sol. Energy Eng*, vol. 124, no. 2, pp. 165–169, 2002, doi: 10.1115/1.1464124.
- [2] M. Binder, C. Schuhbauer, R. Uhlig, P. Schwarzbözl, R. Schwaiger, and R. Pitz-Paal, "Comparison of different safety concepts for evaluation of molten salt receivers," *Solar Energy*, vol. 234, pp. 119–127, 2022, doi: 10.1016/j.solener.2022.01.051.
- [3] D. Hering, M. Binder, P. Schwarzbözl, R. Schwaiger, and R. Pitz-Paal, "Monitoring of service life consumption for tubular solar receivers: Review of contemporary thermomechanical and damage modeling approaches," *Solar Energy*, vol. 226, pp. 427–445, 2021, doi: 10.1016/j.solener.2021.08.022.
- [4] R. Popp, K. Iding, P. Schwarzbözl, T. Konrad, and D. Abel, "A comparison between model predictive and PID-based control of a molten salt solar tower receiver," *AIP Conf. Proc.*, vol. 2815, no. 1, p. 30016, 2023, doi: 10.1063/5.0148728.
- [5] C. Schwager, C. J. T. Boura, R. Flesch, S. Alexopoulos, and U. Herrmann, "Improved efficiency prediction of a molten salt receiver based on dynamic cloud passage simulation," *AIP Conf. Proc.*, vol. 2126, no. 1, p. 30054, 2019, doi: 10.1063/1.5117566.
- [6] C. Schwager, R. Flesch, P. Schwarzbözl, U. Herrmann, and C. J. Teixeira Boura, "Advanced two phase flow model for transient molten salt receiver system simulation," *Solar Energy*, vol. 232, pp. 362–375, 2022, doi: 10.1016/j.solener.2021.12.065.
- [7] C. Schwager, F. Angele, B. Nouri, P. Schwarzbözl, C. J. Teixeira Boura, and U. Herrmann, "Impact of DNI Forecast Quality on Performance Prediction for a Commercial Scale Solar Tower: Application of Nowcasting DNI Maps to Dynamic Solar Tower Simulation," in *SolarPACES Conference 2022*, 2022.